The effect of parallel electric field in shock waves on the acceleration of relativistic ions, electrons, and positrons

Seiichi Takahashi,[1] Hiromasa Kawai,[1] Yukiharu Ohsawa,[1,a)] Shunsuke Usami,[2] Charles Chiu,[3] and Wendell Horton[3]
[1]*Department of Physics, Nagoya University, Nagoya 464-8602, Japan*
[2]*National Institute for Fusion Science, Toki 509-5292, Japan*
[3]*Institute for Fusion Studies, The University of Texas at Austin, Austin, Texas 78712, USA*

(Received 25 August 2009; accepted 27 October 2009; published online 20 November 2009)

The effect of an electric field $E_\parallel$ parallel to the magnetic field $\boldsymbol{B}$ on particle acceleration in shock waves is studied. With test particle calculations, for which the electromagnetic fields of shock waves are obtained from one-dimensional, fully kinetic, electromagnetic, particle simulations, the motions of relativistic ions, electrons, and positrons are analyzed. In these simulations, the shock speed v_{sh} is taken to be close to $c\cos\theta$, where θ is the angle between the external magnetic field and wave normal, and thus strong particle acceleration takes place. Test particle motions calculated in two different methods are compared: In the first method the total electric field $\boldsymbol{E}$ is used in the equation of motion, while in the second method $E_\parallel$ is omitted. The comparison confirms that in the acceleration of relativistic ions $E_\parallel$ is unimportant for high-energy particles. For the acceleration of electrons and positrons, however, $E_\parallel$ is essential. © *2009 American Institute of Physics*.
[doi:10.1063/1.3264739]

I. INTRODUCTION

The ideal magnetohydrodynamics (MHD)[1–3] assumes perfect conductivity, $\boldsymbol{E}+\boldsymbol{v}\times\boldsymbol{B}/c=0$, and it was generally thought that the electric field parallel to the magnetic field, $E_\parallel=(\boldsymbol{E}\cdot\boldsymbol{B})/B$, is quite weak in MHD phenomena in high-temperature plasmas. Recently, however, $E_\parallel$ in nonlinear magnetosonic waves has been analytically obtained and observed with electromagnetic particle simulations,[4] which shows that $E_\parallel$ can be strong and the magnitude of the integral of $E_\parallel$ along the magnetic field (parallel pseudopotential), $F=-\int E_\parallel ds$, is $eF\sim(m_i v_A^2+\Gamma_e T_e)\epsilon$ in shock waves, where m_i is the ion mass, v_A is the Alfvén speed, Γ_e is the specific heat ratio of electrons, T_e is the electron temperature, and ϵ is the amplitude of the shock wave.

The parallel electric field appears in the theories of particle acceleration in shock waves in several different ways; for instance, in the positron acceleration parallel to the magnetic field,[5] the energy increase rate of an accelerated positron is proportional to $E_\parallel$. In the electron acceleration discussed in Ref. 6, the energization and trapping is triggered by the reflection near the end of the main pulse of a shock wave; the reflection can take place when F becomes small there. In contrast, in the theory of incessant acceleration of relativistic ions,[7] the parallel electric field was ignored.

In this paper, we revisit these mechanisms. Bearing the recent work on the parallel electric field[4] in mind, we focus on the effect of $E_\parallel$ on particle motions.

First, in Sec. II, we examine the validity of the approximation ignoring $E_\parallel$ in the theoretical analysis of relativistic ions. We outline the theory of the incessant acceleration of relativistic ions and discuss the contribution of $E_\parallel$. This mechanism works when the shock speed v_{sh} is close to $c\cos\theta$, where θ is the angle between the external magnetic field $\boldsymbol{B}_0$ and the wave normal. (The Alfvén Mach number is about 5 for the parameters $m_i/m_e=1836$, $\cos\theta\sim0.1$, and gyro-to-plasma frequency ratio $|\Omega_e|/\omega_{pe}=1$.) We then perform test particle simulations; that is, we carry out a one-dimensional, fully kinetic, electromagnetic simulation, and then using these electric and magnetic fields and assuming stationary wave propagation, we follow the trajectories of test particles. We calculate test particle orbits in two different ways. In the first method, we integrate the equation of motion with use of total electric field $\boldsymbol{E}$, while in the second method we use the electric field that is perpendicular to the magnetic field, $\boldsymbol{E}_\perp=\boldsymbol{E}-(\boldsymbol{E}\cdot\boldsymbol{B})\boldsymbol{B}/B^2$; i.e., we omit $\boldsymbol{E}_\parallel$ from $\boldsymbol{E}$ in the equation of motion. Comparison of the test particle motions calculated in these two methods shows that the accuracy of the approximation ignoring $E_\parallel$ increases with increasing particle energy, indicating that the previous theoretical treatment[7] is valid.

Next, in Sec. III, we investigate electron and positron motions. The gyroradii of these light particles are usually smaller than the width of the shock transition region, and their cross-field motions are well approximated by the $\boldsymbol{E}\times\boldsymbol{B}$ drift (for the structure of nonlinear magnetosonic waves, see Refs. 8–14). Since the velocity parallel to the magnetic field, $v_\parallel$, is in many cases higher than the $\boldsymbol{E}\times\boldsymbol{B}$ drift velocity, the length $\int v_\parallel dt$ of the light particles in the shock transition region is much greater than the width of the transition region unless the angle θ is small. The work done by the parallel electric field, $\int qE_\parallel v_\parallel dt$, can thus be quite large in magnitude for the light particles. The parallel electric field therefore tends to have much greater effect on the light particles than on the ions.

We follow test electrons and positrons whose initial kinetic energies are of thermal level. Here, we do not assume

a)Electronic mail: ohsawa@nagoya-u.jp.

the stationarity of shock propagation; the electromagnetic fields used for the test particles are exactly the same as the fields obtained in the particle simulation. We consider the case with $v_{sh} \sim c \cos\theta$ again, in which electrons and positrons can be strongly accelerated,[5,6] and calculate test particle orbits by using the total electric field $\boldsymbol{E}$ and by the perpendicular electric field $\boldsymbol{E}_\perp$. In the calculations with $\boldsymbol{E}_\perp$, neither the electron acceleration[6] nor the positron acceleration[5] was observed. In Sec. IV, we summarize our work.

II. RELATIVISTIC IONS

A. Considerations on the effect of parallel electric field

Nonthermal energetic particles with their speeds v higher than the shock speed v_{sh} can move back and forth between the upstream and shock regions in association with their gyromotion. They gain energy from the transverse electric field when they are in the shock wave. If the shock speed v_{sh} is close to $c \cos\theta$, relativistic particles with $v \sim c$ can move with the shock wave for long periods of time and can incessantly repeat this process with their energies going up stepwise.[7]

One can analytically obtain the energy increase in such energetic particles by integrating the equation for the momentum $\boldsymbol{p}$,

$$\frac{d}{dt}\left(\frac{\boldsymbol{p}\cdot\boldsymbol{p}}{2}\right) = q_i \boldsymbol{E}\cdot\boldsymbol{p}, \tag{1}$$

along the unperturbed orbit. Provided that an energetic ion enters a shock wave at $t=t_{in}$ and goes out to the upstream region at $t=t_{out}$ (see Fig. 1), the increment in p^2 in the period $t=t_{out}-t_{in}$ is given as

$$\begin{aligned}\delta\left(\frac{p^2}{2}\right) = {} & q_i p_{1\parallel} E_\parallel (t_{out}-t_{in}) - \frac{2q_i \gamma p_{1\perp}}{\Omega_{i1}}(E_x \sin\theta_1 - E_z \cos\theta_1) \\ & \times \sin\left[-\frac{\Omega_{i1}(t_{out}+t_{in})}{2\gamma}+\eta\right]\sin\left[-\frac{\Omega_{i1}(t_{out}-t_{in})}{2\gamma}\right] \\ & + \frac{2q_i \gamma p_{1\perp}}{\Omega_{i1}} E_y \cos\left[-\frac{\Omega_{i1}(t_{out}+t_{in})}{2\gamma}+\eta\right] \\ & \times \sin\left[-\frac{\Omega_{i1}(t_{out}-t_{in})}{2\gamma}\right],\end{aligned} \tag{2}$$

where, for definiteness, the shock wave is assumed to propagate in the x direction in an external magnetic field $\boldsymbol{B}_0 = B_0(\cos\theta, 0, \sin\theta) = (B_{x0}, 0, B_{z0})$ (for the details of the calculation, see Ref. 7). The quantity Ω_i is the nonrelativistic ion gyrofrequency; the subscript $\perp$ and 1, respectively, refer to vector components perpendicular to $\boldsymbol{B}$ and quantities in the shock wave, where the magnetic field is stronger than in the upstream region; hence, for instance, the x component of the momentum may be expressed as $p_x(t) = p_{1\parallel}\cos\theta_1 + p_{1\perp}\sin\theta_1 \sin(-\Omega_{i1}t/\gamma + \eta)$ in the shock wave region with η the constant in the gyrophase. The parallel electric field can be written as $E_\parallel = E_x \cos\theta_1 + E_z \sin\theta_1$; the contribution of

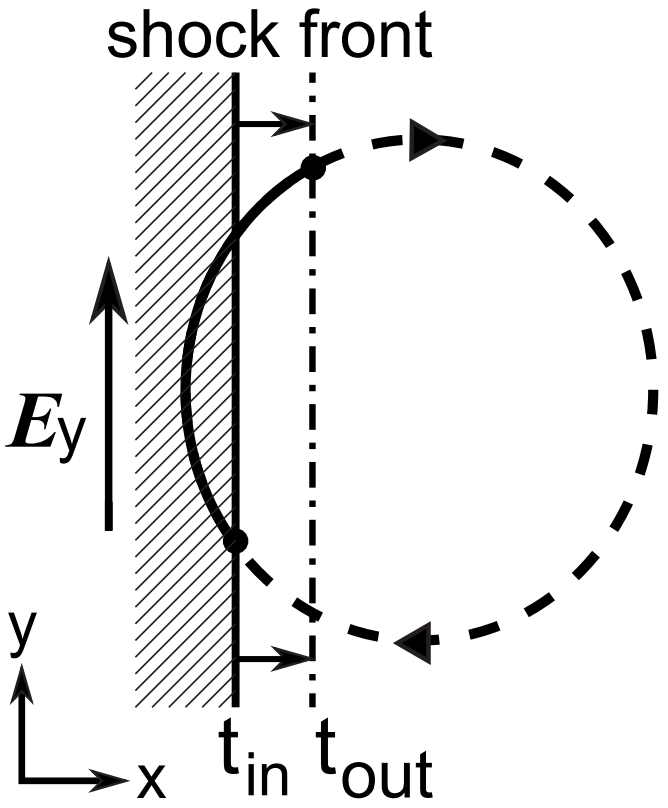

FIG. 1. Schematic diagram of energetic ion orbit. The vertical solid and dotted lines, respectively, show the shock front at $t=t_{in}$ and at $t=t_{out}$. During the period $t=t_{in}$ to t_{out}, the ion is in the shock wave, which propagates in the x direction in an external magnetic field in the (x,z) plane.

B_y is ignored, which is small compared with B_z and B_x. Since $v_{sh} \sim c\cos\theta$, the relation

$$\cos\left[-\frac{\Omega_{i1}(t_{out}+t_{in})}{2\gamma}+\eta\right] \simeq -1, \tag{3}$$

holds for relativistic particles. We then find the increase in γ as

$$\delta\gamma = \frac{2q_i p_{1\perp} E_{1\perp}}{m_i^2 c^2 \Omega_{i1}} \sin\left[\frac{\Omega_{i1}(t_{out}-t_{in})}{2\gamma}\right] + \frac{q_i}{m_i c^2}\int_{t_{in}}^{t_{out}} v_\parallel E_\parallel dt. \tag{4}$$

Equation (4) gives the amount of energy that a fast particle gains in one gyroperiod. In the incessant acceleration, which can occur when $v_{sh} \sim c\cos\theta$, an accelerated particle suffers this energy jump many times in association with its gyromotion. Thus, the time variation in γ resembles a stairway.

The strength of E_y, which is the main part of $\boldsymbol{E}_\perp$ in a large-amplitude magnetosonic wave, $E_y \simeq E_\perp$, is given as[15]

$$\frac{E_{y1}}{B_{z0}} = \frac{\gamma_{sh}^2 v_{sh}}{c}\left[\left(1+\frac{2v_{sh}^2}{v_A^2 \sin^2\theta}\right)^{1/2} - 1\right] = \frac{v_{sh}}{c}\frac{(B_z - B_{z0})}{B_{z0}}, \tag{5}$$

where $\gamma_{sh} = (1 - v_{sh}^2/c^2)^{-1/2}$. In the previous papers,[7] the effect of $E_\parallel$ [the second term on the right-hand side of Eq. (4)] was ignored.

The parallel momentum also increases in the gyromotion owing to the sharp rise of the magnetic field strength in the shock transition region. From the equation of motion, we have

$$\frac{d(\boldsymbol{p}\cdot\boldsymbol{B})}{dt}=\boldsymbol{p}\cdot\frac{d\boldsymbol{B}}{dt}+q_i\boldsymbol{E}\cdot\boldsymbol{B}. \tag{6}$$

If we ignore the second term on the right-hand side of Eq. (6) under the assumption that the parallel electric field is weak, we find the increment in the parallel momentum $p_{0\|}$ measured in the upstream region, $\delta p_\|=p_{0\|}(t_{\rm out})-p_{0\|}(t_{\rm in})$, as

$$\delta p_\|=[\boldsymbol{p}_{1\perp}(t_{\rm out})-\boldsymbol{p}_{1\perp}(t_{\rm in})]\cdot\boldsymbol{B}_0/B_0, \tag{7}$$

which is always positive.[7]

Because of the increase in $v_\|$, particles suffering this acceleration process tend to go away ahead of the shock wave after a few gyroperiods; thus, the acceleration ceases. However, particles can move with the shock wave for long periods of time if $v_{\rm sh}\sim c\cos\theta$, because even if the energy and momentum continue to increase, the particle speed is bounded by the speed of light c (thus, the average particle velocity in the x direction, $v_\|\cos\theta$, remains to be lower than $c\cos\theta$).

The effect of $E_\|$ was ignored in the estimate of $\delta\gamma$ and $\delta p_\|$ in the previous work[7] because it was thought that $E_\|$ was weak in MHD phenomena. Recently, however, it has been recognized that $E_\|$ is much stronger in shock waves than is expected from the ideal MHD theory, in which $E_\|=0$. The magnitude of the parallel pseudopotential, $F=-\int E_\| ds$, is found to be

$$eF\sim(m_iv_{\rm A}^2+\Gamma_eT_e)\frac{(B_z-B_{z0})}{B_0}, \tag{8}$$

for shock waves, and the parallel electric field is

$$E_\|\sim\frac{(m_iv_{\rm A}^2+\Gamma_eT_e)B_{x0}}{(c/\omega_{pi})eB_1}\frac{(B_z-B_{z0})}{B_0}$$
$$=\frac{v_{\rm A}}{c}\left(1+\frac{c_{se}^2}{v_{\rm A}^2}\right)\frac{B_{x0}}{B_1}(B_z-B_{z0}), \tag{9}$$

where $c_{se}=(\Gamma_eT_e/m_i)^{1/2}$.[4] Comparison of Eqs. (5) and (9) shows that $E_\|/E_\perp\sim(v_{\rm A}/v_{\rm sh})(B_{x0}/B_1)$, if $c_{se}^2/v_{\rm A}^2\lesssim1$.

The above discussion suggests that the accuracy of the approximation ignoring the parallel electric field should be better for higher energy particles. The second term on the right-hand side of Eq. (4), which represents the effect of $E_\|$, should become less important as γ rises because $p_{1\perp}$ in the first term is proportional to γ. This is also the case with the right-hand side of Eq. (6): the magnitude of the first term increases with increasing γ, while the second term $(q_i\boldsymbol{E}\cdot\boldsymbol{B})$ is independent of γ.

B. Test particle simulations for relativistic ions

Here, we investigate test particle orbits of energetic ions that encounter a shock wave. To do this, we first carry out a shock wave simulation with a one-dimensional, fully kinetic, electromagnetic particle code,[16,17] and obtain the data of the electric and magnetic fields of the shock wave. Then, assuming that the shock wave propagates steadily, we follow test particle orbits of energetic ions using these field data.

To examine the effect of the parallel electric field, we compute test particle orbits in two different ways. In the first method, we integrate the normal relativistic equation of motion,

$$\frac{d\boldsymbol{p}}{dt}=e\boldsymbol{E}+e\frac{\boldsymbol{v}\times\boldsymbol{B}}{c}, \tag{10}$$

while in the second method we use the perpendicular electric field $\boldsymbol{E}_\perp$ in the equation of motion,

$$\frac{d\boldsymbol{p}}{dt}=e\boldsymbol{E}_\perp+e\frac{\boldsymbol{v}\times\boldsymbol{B}}{c}. \tag{11}$$

We then compare the motions obtained by these two methods.

We take the following parameters for particle simulations. The ion-to-electron mass ratio is $m_i/m_e=400$; the speed of light is $c/(\omega_{pe}\Delta_g)=10$, where Δ_g is the grid spacing; the strength of the external magnetic field is $|\Omega_e|/\omega_{pe}=3.1$ with $\boldsymbol{B}_0=B_0(\cos\theta,0,\sin\theta)$ with $\theta=60°$. The Alfvén speed is thus $v_{\rm A}/(\omega_{pe}\Delta_g)=1.55$. We use the bounded plasma model;[18] the total grid size is $L=16\,384\Delta_g$, and the plasma particles are confined in the region $400\Delta_g<x<15984\Delta_g$, being specularly reflected at these boundaries.

Figure 2 shows the profiles of the electric and magnetic fields of a shock wave obtained from a particle simulation. The shock wave propagates in the x direction with a speed $v_{\rm sh}=3.2v_{\rm A}$. The profiles shown in Fig. 2 are the ones averaged over time. That is, from a shock simulation, we measure the shock speed $v_{\rm sh}$. Then, we take the sum of the field data at times t_j $(j=1,2,\cdots,n)$ as, for instance,

$$\langle B_z(x-v_{\rm sh}t)\rangle=\frac{1}{n}\sum_{j=1}^{n}B_z(x-v_{\rm sh}t_j,t_j). \tag{12}$$

Using these time-averaged field data, we calculate test particle orbits. The test particles are initially in the upstream region with the momentum distribution function

$$f(\boldsymbol{p})=\frac{N}{4\pi p_0^2}\delta(p-p_0), \tag{13}$$

where N is the number of test particles, and p_0 is related to the initial Lorentz factor through $\gamma_0=[1+p_0^2/(m_i^2c^2)]^{1/2}$. The gyroradius of an energetic ion is quite large. In the present parameters, it is $\sim5.2\times10^4\Delta_g$ for $\gamma=40$, which is much greater than the size of the bounded plasma model, $400\Delta_g<x<15\,984\Delta_g$. The fields outside this region are set to be constant, $\boldsymbol{E}=0$ and $\boldsymbol{B}=(B_{x0},0,B_{z0})$, in the test ion calculations.

The upper panel of Fig. 3 compares the time variations in the positions $(x-v_{\rm sh}t)$ of an incessantly accelerated energetic ion with an initial energy $\gamma_0=40$. The solid and dotted lines, respectively, represent the positions that have been obtained with use of the total electric field, Eq. (10), and the positions obtained with use of the perpendicular electric field, Eq. (11); after the encounter with the shock wave, this particle moves with the shock wave crossing the shock tran-

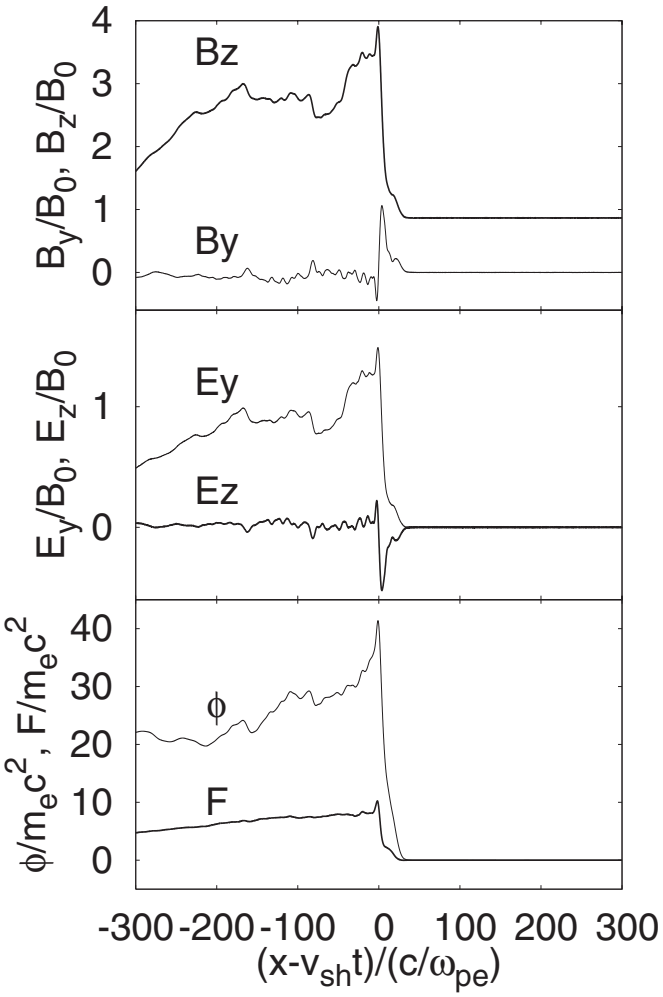

FIG. 2. Time-averaged field profiles obtained from a particle simulation. These fields are used for test particle calculations.

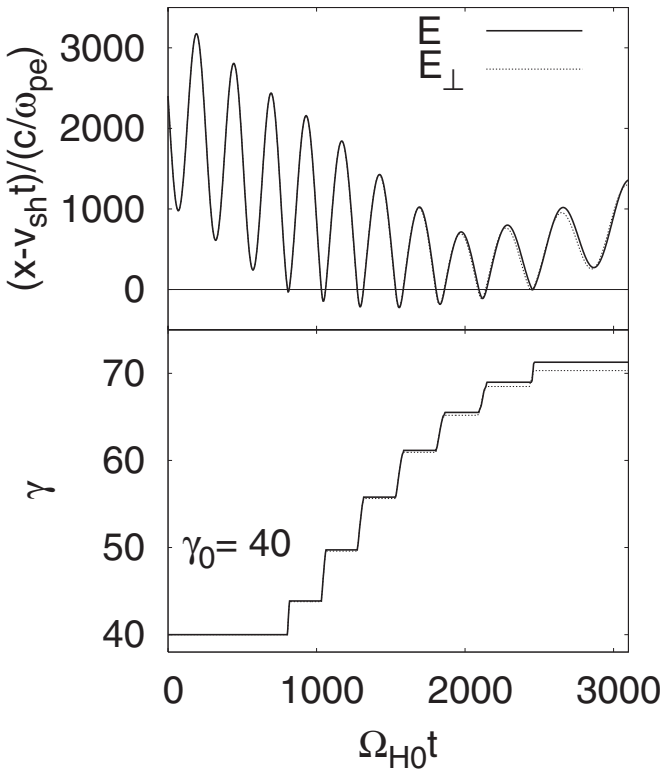

FIG. 3. Time variations in $(x-v_{sh}t)$ and γ. The solid and dotted lines, respectively, show the values calculated with use of $\boldsymbol{E}$ and with $\boldsymbol{E}_\perp$. In the present case (γ_0=40), the solid and dotted lines are quite close.

sition region 14 times and hence suffering energy jumps seven times. We do not find much difference between these two motions, which indicates that the parallel electric field is unimportant in the motion of energetic ions, as suggested in Refs. 7. The lower panel shows the Lorentz factors calculated in these two manners. The two Lorentz factors exhibit quite similar behavior, and their difference $\gamma-\gamma_\perp$, where $\gamma_\perp$ is the Lorentz factor obtained from $\boldsymbol{E}_\perp$, is quite small; $(\gamma-\gamma_\perp)/\gamma=1.4\times10^{-2}$ immediately after the seventh jump.

Figure 4 shows the time variations in the fields $E_\perp$, $E_\parallel$, and B_z that this particle felt. The time variations reflect the fact that strong $E_\perp$ and B_z exist in the shock wave, while $E_\parallel$ is weaker than them and appreciable only in the shock transition region. The energetic particles thus feel $E_\parallel$ for only short periods of time, which also makes the effect of $E_\parallel$ on energetic particles weak.

Figure 5 shows the time variations in the positions and Lorentz factors of a particle with a lower initial energy γ_0 =5. The solid and dotted lines exhibit similar profiles also in this case. Their difference is, however, slightly greater than the previous case with γ_0=40; the ratio $(\gamma-\gamma_\perp)/\gamma$ is 5.9 $\times10^{-2}$ immediately after the seventh jump, which is four times as large as that for γ_0=40. This is consistent with the prediction that the effect of $E_\parallel$ becomes less important (thus, the accuracy of the theory ignoring $E_\parallel$ is improved) as γ increases.

Next, we discuss statistical data of 30 000 test particles. Some particles do not experience energy jumps. Particles with $v_\parallel\cos\theta>v_{sh}$ move faster in the x direction than the shock wave; thus, they do not encounter it if they are initially in the far upstream region. The number of such particles is

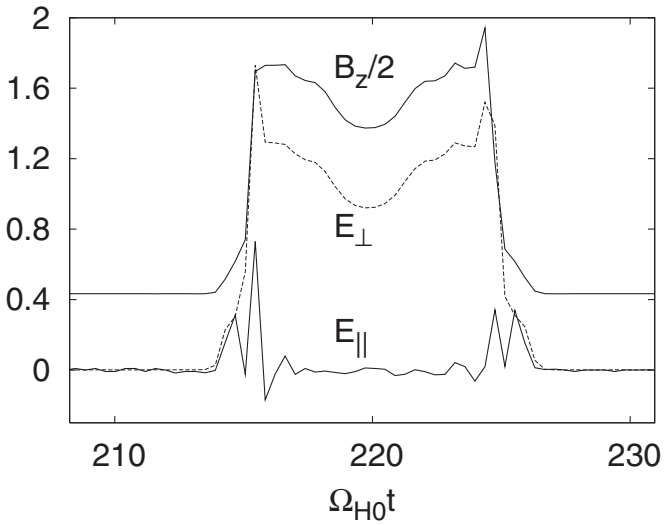

FIG. 4. Time variations in $E_\perp$, $E_\parallel$, and B_z that the particle felt. These quantities are normalized to B_0. The parallel electric field $E_\parallel$ is present only in the shock transition region, while $E_\perp$ and B_z are present in a much larger region behind the shock front.

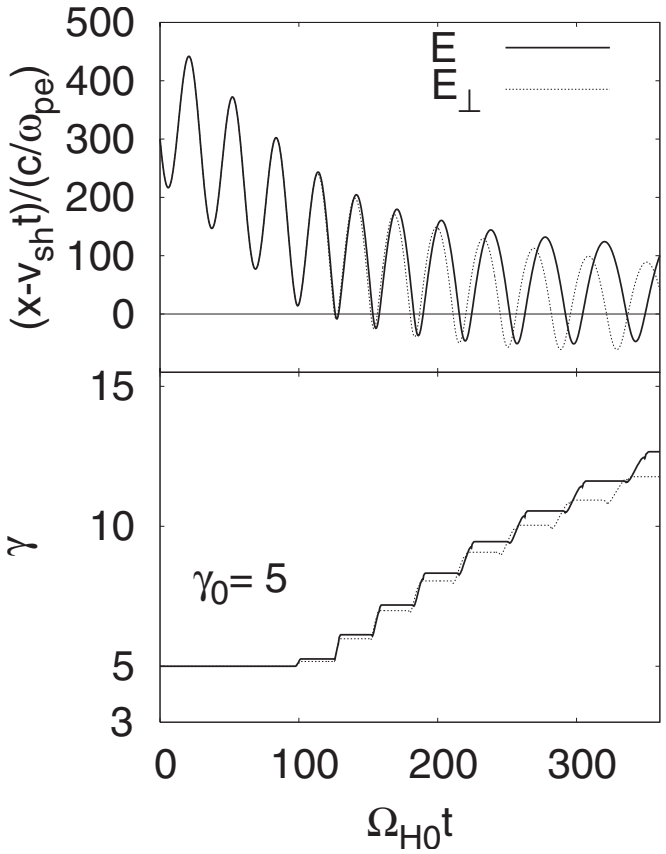

FIG. 5. Time varations in $(x-v_{sh}t)$ and γ calculated with $\boldsymbol{E}$ (solid line) and with $\boldsymbol{E}_\perp$ (dotted line). The differences of the solid and dotted lines are more appreciable in this lower energy case ($\gamma_0=5$) than the previous higher energy case ($\gamma_0=40$).

rather small: For the case with $\gamma_0=40$ calculated with $\boldsymbol{E}$, it was 308. Particles with $v_\parallel \cos\theta < v_{sh}$ encounter the shock wave. A significant fraction of these particles cross the shock transition region only once; they do not return to the upstream region after entering the shock wave. The number of such particles was about 28 000 for $\gamma_0=40$ with $\boldsymbol{E}$. These two types of particles do not experience energy jumps. Figure 6 shows the number of particles N_k that have suffered the

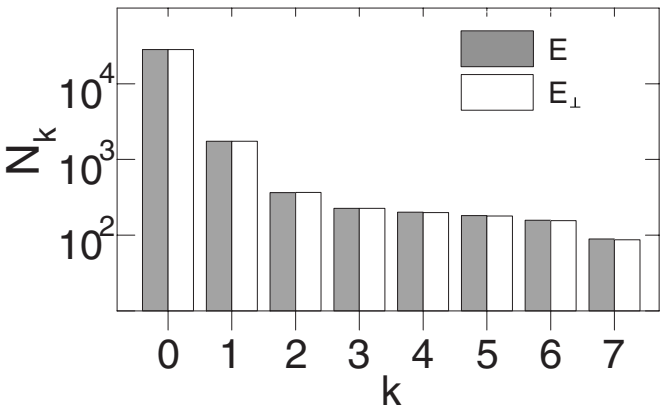

FIG. 6. Particle number N_k as a function of the number of energy jumps k. Here, N_k is the number of particles that have experienced the energy jumps k times or more. The value of N_k decreases rapidly as k increases from $k=0$ to 2, while its decrease is rather slow for $k\geq 2$.

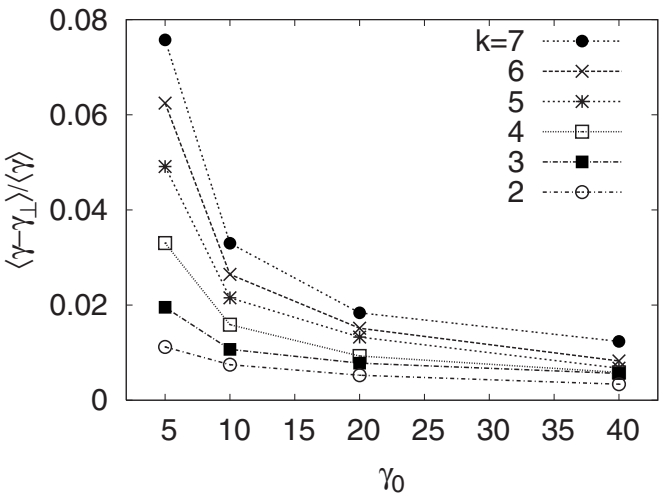

FIG. 7. Energy difference $\langle\gamma-\gamma_\perp\rangle/\langle\gamma\rangle$ vs initial energy γ_0. Here, k is the number of energy jumps that the particles have suffered. For all values of k, $\langle\gamma-\gamma_\perp\rangle/\langle\gamma\rangle$ decreases with increasing γ_0.

energy jumps k times or more; the shaded and white columns represent N_k calculated with $\boldsymbol{E}$ and with $\boldsymbol{E}_\perp$, respectively. In this example, $\boldsymbol{E}$ and $\boldsymbol{E}_\perp$ give nearly the same N_k, and N_k rapidly decreases as k varies from 0 to 2 ($N_2/N_0=0.013$) while for $k\geq 2$ its variation is rather slow.

We now examine the energy dependence of the difference $\gamma-\gamma_\perp$ averaged over test particles. Let $\langle\gamma(k)\rangle$ designate the average Lorentz factor of particles immediately after having suffered the kth energy jump:

$$\langle\gamma(k)\rangle = \frac{1}{N_k}\sum_{j=1}^{N_k}\gamma_j(k). \tag{14}$$

Then, we compare the average energies $\langle\gamma(k)\rangle$ and $\langle\gamma_\perp(k)\rangle$. Figure 7 shows the ratio $\langle\gamma(k)-\gamma_\perp(k)\rangle/\langle\gamma(k)\rangle$ as a function of the initial energy γ_0. The values of the six lines, which represent the cases with $k=2,3,\ldots 7$, decrease with γ_0, indicating that the effect of $E_\parallel$ becomes less important with increasing particle energy. For $\gamma_0=40$, the ratio is quite small, $\langle\gamma(k)-\gamma_\perp(k)\rangle/\langle\gamma(k)\rangle \lesssim 0.012$.

III. ELECTRONS AND POSITRONS

The gyroradii of thermal electrons and positrons are usually much smaller than the width of the shock transition region (for the studies of plasmas containing positrons, see, for instance, Refs. 19–26 and references therein). The $\boldsymbol{E}\times\boldsymbol{B}$ drift is thus a good approximation for both of them. With regard to the motion along the magnetic field, $E_\parallel$ will have much stronger effect on these light particles than on the ions. The parallel velocity $v_\parallel$ of the light particles are in many cases higher than the $\boldsymbol{E}\times\boldsymbol{B}$ drift velocity. They therefore move a long way along the magnetic field when crossing the shock transition region. (For the energetic ions discussed in Sec. II, cross-field motions were important.) In fact, the integral $\int v_\parallel dt$ of the light particles passing through the shock transition region should be $\sim v_\parallel/v_{sh}$ times as long as the width of the transition region, $\sim c/\omega_{pi}$, if $v_\parallel B_{x0}/B < v_{sh}$; the particle will pass through the shock transition region in a

time $\sim(c/\omega_{pi})/v_{sh}$ in this case. [If $v_{\|}B_{x0}/B > v_{sh}$, then $\int v_{\|}dt \sim (B/B_{x0})(c/\omega_{pi})$.] The work done by the parallel electric field, $\int qE_{\|}v_{\|}dt$, on the light particles would thus become much greater than that on the ions.

Furthermore, $E_{\|}$ pushes the positrons in the direction opposite to that of the electrons; it acts to reflect positrons along the magnetic field from the shock transition region where the parallel pseudopotential F rises, while $E_{\|}$ acts to pull electrons into the shock wave. Comparison of positron and electron motions will therefore clearly show the effect of $E_{\|}$.

With these considerations in mind, we study the effect of $E_{\|}$, comparing the motions of these two particle species in shock waves. As in Sec. II, we consider shock waves with $v_{sh} \sim c\cos\theta$, for which there are important acceleration mechanisms for electrons and for positrons.[5,6] That is, some electrons are reflected near the end of the main pulse region of a shock wave and then accelerated and trapped in the main pulse region. Positrons can be accelerated along the magnetic field with the energy increase rate

$$\frac{1}{\Omega_{p0}}\frac{d\gamma}{dt} = \frac{c\cos\theta}{v_{sh}}\frac{(\boldsymbol{E}\cdot\boldsymbol{B})}{(\boldsymbol{B}\cdot\boldsymbol{B}_0)}, \tag{15}$$

where Ω_{p0} is the nonrelativistic positron gyrofrequency in the upstream region.

A. Particle simulations with test particles

We carry out one-dimensional, fully kinetic, electromagnetic particle simulations for a plasma consisting of ions, electrons, and positrons with the positron-to-electron density ratio $n_{p0}/n_{e0}=0.02$; other plasma parameters for the particle simulations are the same as those in Sec. II B. In addition to these plasma particles, we initially put a bunch of test positrons and electrons at some location in the upstream region with the momentum distribution function [Eq. (13)]. Their initial kinetic energy is thermal level; $\gamma_0=1.0037$ $[v/(\omega_{pe}\Delta_g)=c(1-\gamma_0^{-2})^{1/2}/(\omega_{pe}\Delta_g)=0.86]$. These test particles move according to the fields created by the plasma particles. The charges and currents of the test particles, however, do not affect the plasma behavior. This simulation differs from the ones in Sec. II B in that the shock wave in the test particle calculation is not assumed to be stationary: as the plasma particles, they feel the fields that vary with time and space and are confined in the simulation box of the bounded plasma model. We can perform this type of test particle calculations because the positrons and electrons are much lighter than the ions; thus, the simulation time is much shorter. As in Sec. II B, we calculate test particle trajectories in two ways; i.e., with use of $\boldsymbol{E}$ and with $\boldsymbol{E}_{\perp}$.

1. Electron motion

Figure 8 shows the profiles of B_z and phase spaces (x,γ) of test electrons for a shock wave with a propagation speed $v_{sh}/(\omega_{pe}\Delta_g)=4.7$, which is close to the value $c\cos\theta/(\omega_{pe}\Delta_g)=5$. By this time $(\omega_{pe}t=2000)$, all the test particles have entered the shock wave from the upstream region. In the upper panel, in which the total electric field $\boldsymbol{E}$ was used to calculate test particle motions, some electrons have been trapped and are near the shock front with ultrarelativistic energies $\gamma\sim100$, while in the lower panel, in which $\boldsymbol{E}_{\perp}$ was used, we do not find very high-energy electrons. This is because, in the absence of $E_{\|}$, particle reflection caused by the dip of the parallel pseudopotential F in the end of the main pulse region does not occur. (In the lower panel, there are a few particles with $\gamma\sim60$. This energization mechanism is different from the one in the upper panel and is described below in Fig. 11.)

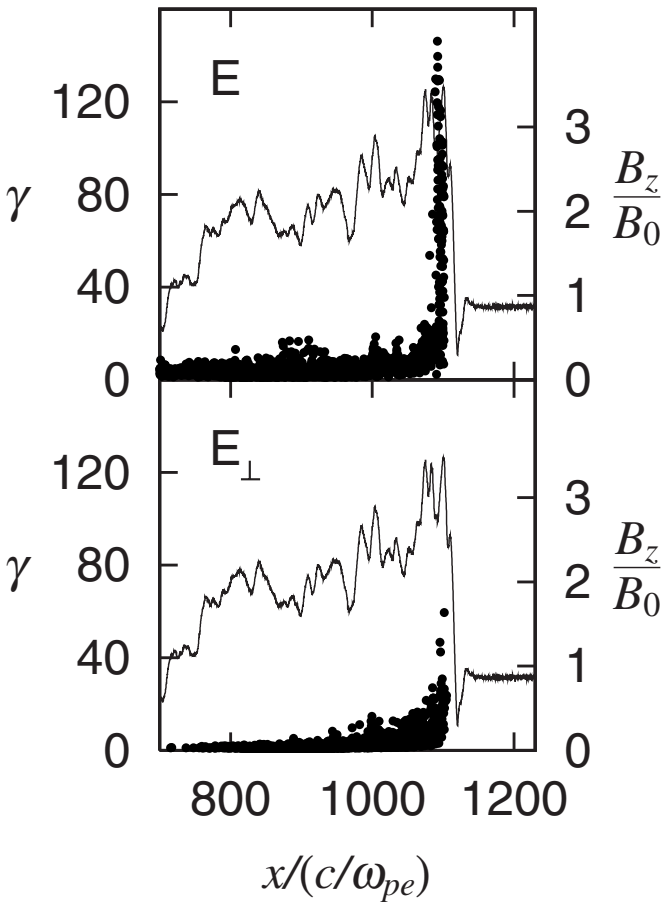

FIG. 8. Profiles of B_z and phase spaces (x,γ) of test electrons. The initial energy of the test electrons is thermal level, $\gamma_0=1.0037$. In the upper panel, in which the total electric field $\boldsymbol{E}$ was used in the equation of motion for the test electrons, high-energy electrons with $\gamma\sim100$ are present, while in the lower panel, in which the perpendicular electric field $\boldsymbol{E}_{\perp}$ was used, there are no electrons with $\gamma\sim100$.

Figure 9 shows two electron orbits in the $(x-v_{sh}t,y)$ plane; even though the initial positions and velocities of these test particles are exactly the same, the particle calculated with $\boldsymbol{E}$ (thick line) is reflected near the end of the main pulse of the shock wave and trapped in the main pulse region, while the particle calculated with $\boldsymbol{E}_{\perp}$ (thin line) passes through this region without strong interactions with the shock wave. Figure 10 displays the time variations in the positions $(x-v_{sh}t,y,z)$ and Lorentz factors γ of these electrons. The quantity $(x-v_{sh}t)$ of the accelerated electron (thick line) stops decreasing when it is reflected at $\omega_{pe}t=630$, and $(x-v_{sh}t)$, y, and γ begin to oscillate with a period $\omega_{pe}t\sim1100$, which is much longer than the relativistic gyroperiod with $\omega_{pe}t\lesssim40$. Figures 9 and 10 verify that the particle

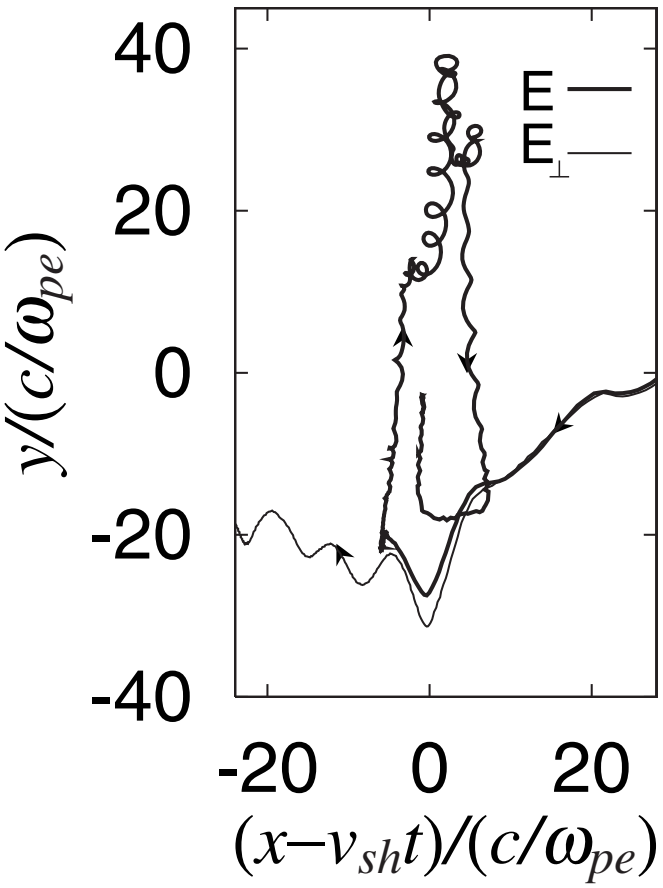

FIG. 9. Trajectories of a test electron calculated with $\boldsymbol{E}$ (thick line) and that with $\boldsymbol{E}_\perp$ (thin line). Although their initial positions and velocities are exactly the same, the former particle is trapped in the main pulse region, while the latter passes through it.

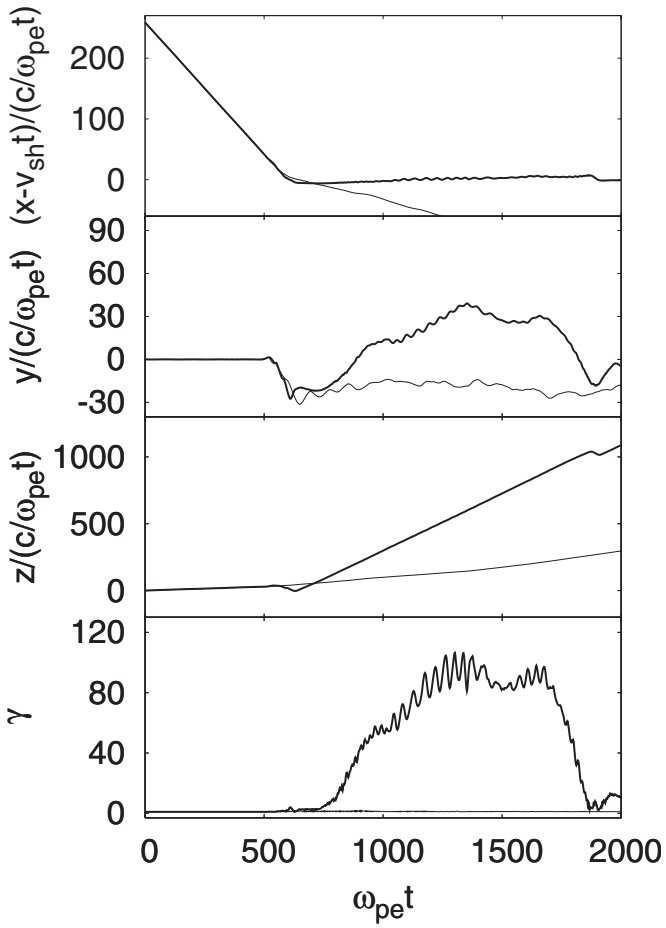

FIG. 10. Time variations in the positions and energies of the test electron calculated with $\boldsymbol{E}$ (thick line) and that with $\boldsymbol{E}_\perp$ (thin line). The former particle is trapped, and its $(x-v_{sh}t)$, y, and γ oscillate.

depicted by the thick lines was accelerated by the mechanism discussed in Ref. 6 and that this acceleration does not take place if $\boldsymbol{E}_\perp$ is used in the calculations.

Figure 11 shows the case in which the shock speed $[v_{sh}/(\omega_{pe}\Delta_g)=4.3]$ is slightly lower than the previous one; and thus the difference $(c\cos\theta - v_{sh})$ is larger. There are a significant number of high-energy electrons in the lower panel (calculated with $\boldsymbol{E}_\perp$) as well as in the upper panel (calculated with $\boldsymbol{E}$). The acceleration mechanism in the upper panel is the same as that in the upper panel of Fig. 8, while the energization in the lower panel is due to the $-\mu\nabla B$ force, where μ is the magnetic moment. This force acts to reflect particles from the shock front to the upstream region because the magnetic pressure is much higher in the shock wave than in the upstream region, while the parallel electric field acts to pull electrons into the shock wave from the upstream region. If there is no parallel electric field, therefore, electron reflection is enhanced. We thus have high-energy electrons in the lower panel of Fig. 11. (Since the shock speed is lower in Fig. 11 than in Fig. 8, electron reflection is easier to occur.)

Figure 12 shows the orbit in the $(x-v_{sh}t, y)$ plane of an electron calculated with $\boldsymbol{E}_\perp$, and Fig. 13 displays the time variations in the position and energy of this particle. This particle continues to gyrate in the shock transition region, with its guiding center slowly moving along the shock front and its energy going up. It is noted, however, that if the total $\boldsymbol{E}$ is used in the calculations, this type of acceleration rarely occurs in thermal electrons.

2. Positron motion

Figure 14 shows the profiles of B_z and phase spaces (x,γ) of test positrons at $\omega_{pe}t=2000$ for a shock wave with $v_{sh}/(\omega_{pe}\Delta_g)=4.7$. The upper panel (calculated with $\boldsymbol{E}$) indicates that most of the positrons stay near the shock front after meeting the shock wave and some of them have been accelerated to energies $\gamma\sim 300$, while the lower panel (calculated with $\boldsymbol{E}_\perp$) shows that all the positrons have moved or are moving to the downstream region with their γ's being low. We thus clearly see that the parallel electric field plays an essential role in the positron motions. The acceleration mechanism in the upper panel is the one studied in Ref. 5, in which the energy increase rate [Eq. (15)], which is proportional to $E_\parallel$, was given.

Figure 15 shows the case in which the shock propagation speed is slightly lower, $v_{sh}/(\omega_{pe}\Delta_g)=4.3$. In the upper panel (calculated with $\boldsymbol{E}$), there are high-energy positrons near the shock front; the maximum positron energy ($\gamma\sim 150$) is, however, approximately a half of that in Fig. 14. Some positrons are reflected at the shock front and then go away ahead of the

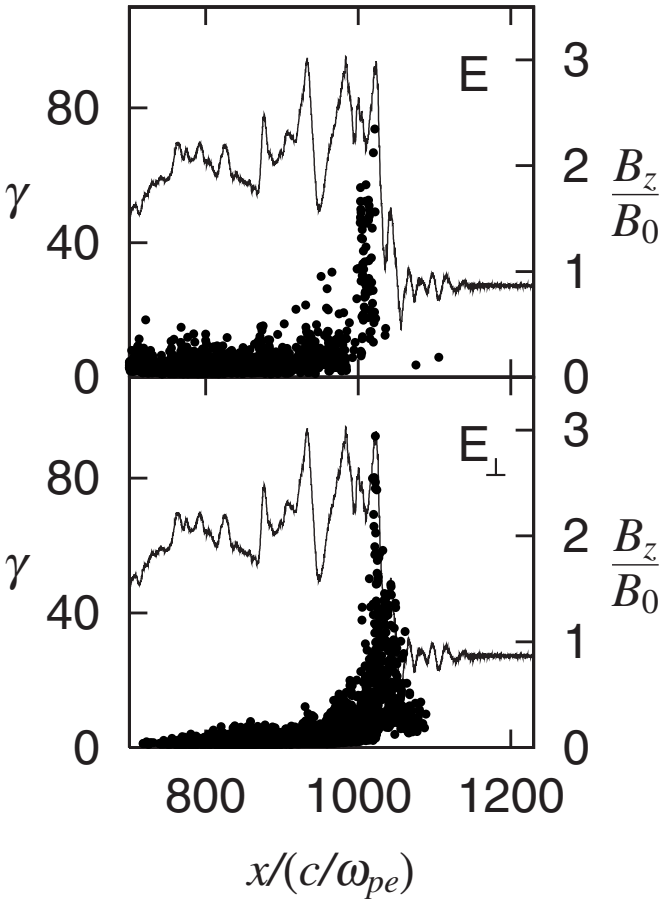

FIG. 11. Profiles of B_z and phase spaces (x,γ) of test electrons for a shock wave with a slower propagation speed $v_{sh}/(\omega_{pe}\Delta_g)=4.3$. High-energy electrons with $\gamma\sim 100$ are present near the shock front in both panels.

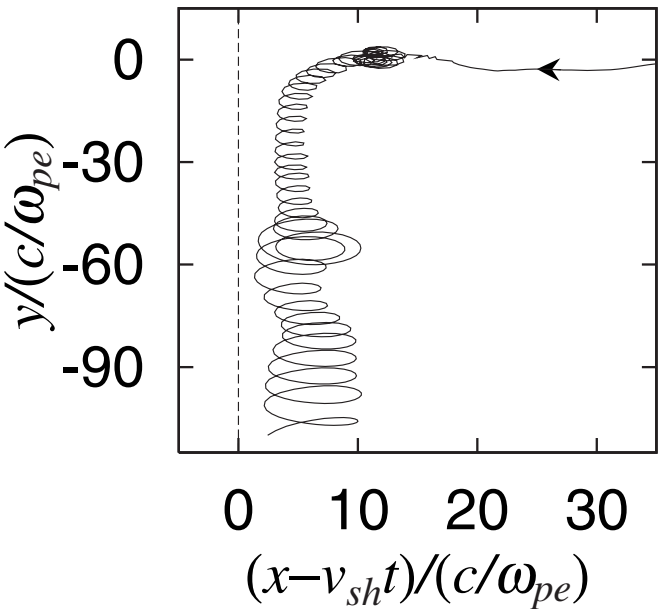

FIG. 12. Trajectory of a test electron calculated with $\boldsymbol{E}_\perp$. The vertical dotted line $(x-v_{sh}t=0)$ indicates the position at which B_z takes its maximum value. After the encounter with the shock wave, this particle moves along the shock front, keeping the gyration.

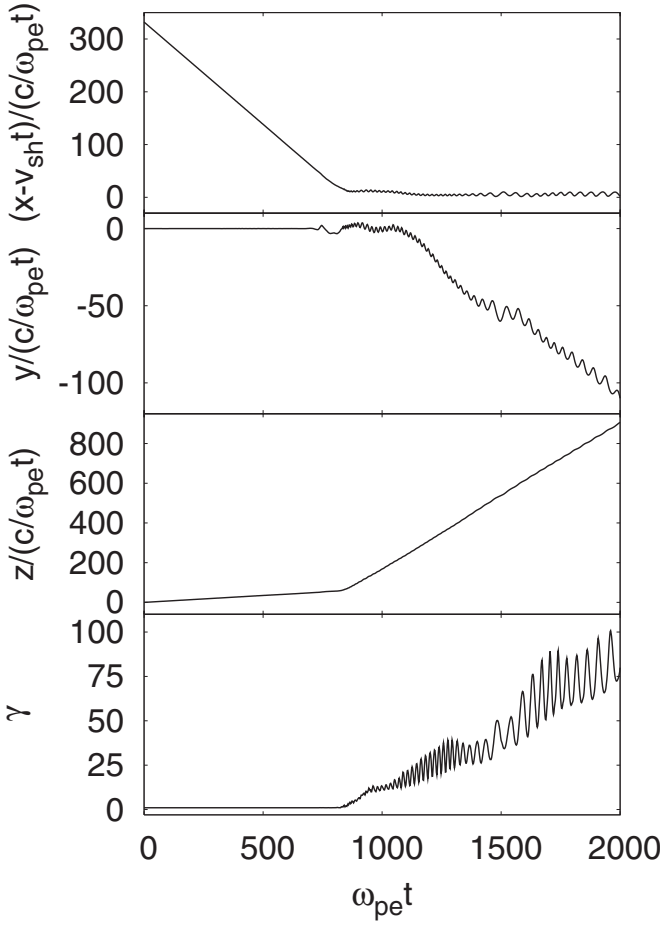

FIG. 13. Time variations in the position and energy of the test particle shown in Fig. 12. The Lorentz factor γ increases after this particle met the shock wave at $\omega_{pe}t=810$.

shock wave. These two points are due to the fact that the shock speed is lower. In the lower panel (calculated with $\boldsymbol{E}_\perp$), we find some positrons near the shock front. Their maximum energy is comparable to that of the electrons in the lower panel of Fig. 11. As those electrons, positrons can be pushed forward by the $-\mu\nabla B$ force in the absence of the parallel electric field.

Finally, we note that the initial energies of the above test electrons and positrons were thermal level. If their initial energies are so high that their gyroradii are greater than the shock width, the acceleration process observed in relativistic ions, in which $\boldsymbol{E}_\perp$ is more important than $\boldsymbol{E}_\parallel$, could occur.

IV. SUMMARY

We have studied the effect of the electric field parallel to the magnetic field, $E_\parallel$, on particle motions in shock waves by using computer simulations. This work was motivated by the recent discovery that $E_\parallel$ can be quite strong in nonlinear magnetosonic waves.[4] Specifically, we have examined the motions of relativistic ions, electrons, and positrons for the case $v_{sh}\sim c\cos\theta$, for which strong acceleration mechanisms operate.

In the previous theoretical analysis[7] of the acceleration of relativistic ions that have speeds higher than v_{sh} and gyroradii far exceeding the width of the shock transition region,

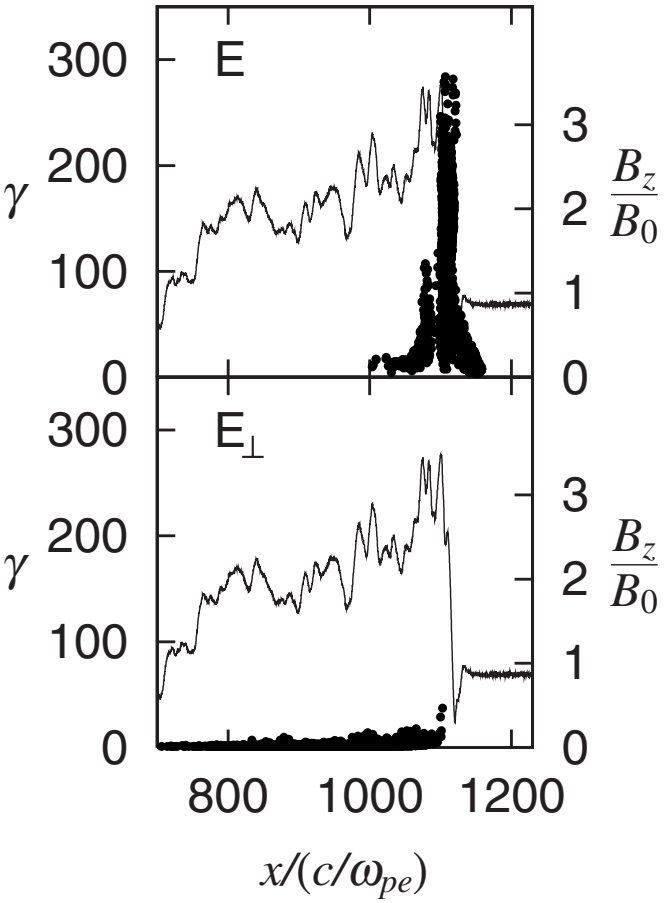

FIG. 14. Profiles of B_z and test positron phase spaces (x,γ) for a shock wave with $v_{sh}/(\omega_{pe}\Delta_g)=4.7$. In the upper panel calculated with $\boldsymbol{E}$ there are many ultrarelativistic positrons, while in the lower panel calculated with $\boldsymbol{E}_\perp$ most of the positrons have moved to the downstream region with low energies.

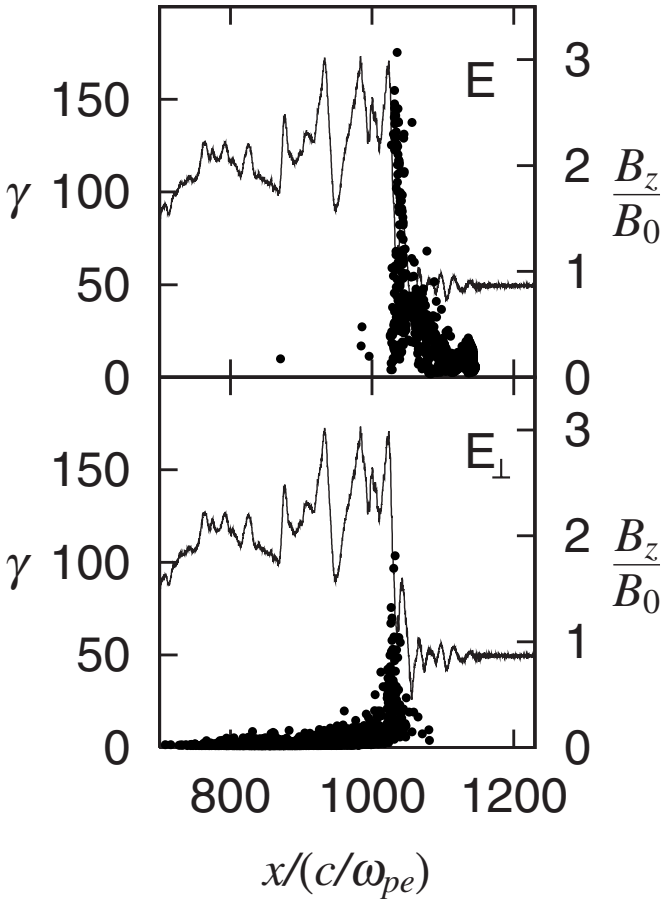

FIG. 15. Profiles of B_z and phase spaces of test positron (x,γ) for a shock wave with $v_{sh}/(\omega_{pe}\Delta_g)=4.3$. The maximum energy in the upper panel is about a half of that in the case of $v_{sh}/(\omega_{pe}\Delta_g)=4.7$. The phase space in the lower panel is quite similar to that of the electrons in the lower panel of Fig. 11.

the parallel electric field was ignored. Here, we have numerically discussed the validity of the theoretical treatment ignoring $E_\parallel$; i.e., we have carried out shock simulations with a fully kinetic, electromagnetic, particle code, and then using these electromagnetic data and assuming stationary wave propagation, we have followed the trajectories of test particles (relativistic ions) coming from the upstream region. In calculating the orbits, we have used two methods: In the first method we have used the total electric field $\boldsymbol{E}$ in the equation of motion for the test particles, while in the second method we have used the perpendicular electric field $\boldsymbol{E}_\perp$. By comparing the results of these two methods, we have evaluated the effect of $E_\parallel$ and confirmed that the approximation ignoring $E_\parallel$ is valid when the particle energy γ is sufficiently high.

In contrast to the energetic ions, the parallel electric field has strong effect on electrons and positrons. We have performed fully kinetic, electromagnetic, particle simulations for a three-component plasma consisting of ions, electrons, and low-density positrons with $n_{p0}/n_{e0}=0.02$. In these simulations, we have also calculated the motions of test electrons and positrons, which do not affect the plasma behavior; again, for one test particle group, we used the total electric field $\boldsymbol{E}$ in the equation of motion, and for the other, we used the perpendicular electric field $\boldsymbol{E}_\perp$. The initial energies of the test particles were taken to be thermal level. It has been demonstrated that the electron acceleration studied in Ref. 6, in which the formation of the dip of the parallel pseudopotential F triggers the trapping and acceleration, does not occur in the test electrons calculated with $\boldsymbol{E}_\perp$. It has also been shown that the positron acceleration studied in Ref. 5 does not occur in the absence of $E_\parallel$. In addition, the test particle calculations with $\boldsymbol{E}_\perp$ enabled us to see the effects that are usually masked by the strong effect of $E_\parallel$, deepening our understanding of particle motions.

ACKNOWLEDGMENTS

This work was carried out by the joint research program of the Solar-Terrestrial Environment Laboratory, Nagoya University, and by the collaboration program, Grant No. NIFS09KTAN006, of the National Institute for Fusion Science, and was supported in part by the Grant-in-Aid for Scientific Research (C) Grant No. 20540481 of the Japan Society for the Promotion of Science, by the U.S.-Japan Joint Institute for Fusion Theory, and by the U.S. NSF Grant No. ATM-0638480.

[1]H. Alfvén and C.-G. Fälthammer, *Cosmical Electrodynamics* (Clarendon, Oxford, 1963).
[2]D. Biskamp, *Magnetic Reconnection in Plasmas* (Cambridge University Press, Cambridge, 2000).
[3]J. V. Hollweg, Astrophys. J. **277**, 392 (1984).
[4]S. Takahashi and Y. Ohsawa, Phys. Plasmas **14**, 112305 (2007); S. Takahashi, M. Sato, and Y. Ohsawa, *ibid.* **15**, 082309 (2008).
[5]H. Hasegawa, S. Usami, and Y. Ohsawa, Phys. Plasmas **10**, 3455 (2003); H. Hasegawa, K. Kato, and Y. Ohsawa, *ibid.* **12**, 082306 (2005).
[6]N. Bessho and Y. Ohsawa, Phys. Plasmas **6**, 3076 (1999); **9**, 979 (2002).
[7]S. Usami and Y. Ohsawa, Phys. Plasmas **9**, 1069 (2002); **11**, 3203 (2004).
[8]J. H. Adlam and J. E. Allen, Philos. Mag. **3**, 448 (1958).
[9]L. Davis, R. Lüst, and A. Schlüter, Z. Naturforsch. A **13**, 916 (1958).
[10]R. Z. Sagdeev, in *Reviews of Plasma Physics*, edited by M. A. Leontovich (Consultants Bureau, New York, 1966), Vol. 4, pp. 23–91.
[11]C. S. Gardner and G. K. Morikawa, Commun. Pure Appl. Math. **18**, 35 (1965).
[12]T. Kakutani, H. Ono, T. Taniuti, and C. C. Wei, J. Phys. Soc. Jpn. **24**, 1159 (1968).
[13]T. Kakutani and H. Ono, J. Phys. Soc. Jpn. **26**, 1305 (1969).
[14]Y. Ohsawa, Phys. Fluids **29**, 1844 (1986); **29**, 2474 (1986).
[15]S. Miyahara, T. Kawashima, and Y. Ohsawa, Phys. Plasmas **10**, 98 (2003).
[16]A. B. Langdon and C. K. Birdsall, Phys. Fluids **13**, 2115 (1970).
[17]P. C. Liewer, A. T. Lin, J. M. Dawson, and M. Z. Caponi, Phys. Fluids **24**, 1364 (1981).
[18]Y. Ohsawa, Phys. Fluids **28**, 2130 (1985).
[19]P. A. Sturrock, Astrophys. J. **164**, 529 (1971).
[20]C. F. Kennel and R. Pellat, J. Plasma Phys. **15**, 335 (1976).
[21]J.-I. Sakai and T. Kawata, J. Phys. Soc. Jpn. **49**, 753 (1980).
[22]J. N. Leboeuf, M. Ashour-Abdalla, T. Tajima, C. F. Kennel, F. V. Coroniti, and J. M. Dawson, Phys. Rev. A **25**, 1023 (1982).
[23]G. S. Lakhina and F. Verheest, Astrophys. Space Sci. **253**, 97 (1997).
[24]G. A. Stewart and E. W. Laing, J. Plasma Phys. **47**, 295 (1992).
[25]C. S. Reynolds, A. C. Fabian, A. Celotti, and M. J. Rees, Mon. Not. R. Astron. Soc. **283**, 873 (1996).
[26]K. Hirotani, S. Iguchi, M. Kimura, and K. Wajima, Publ. Astron. Soc. Jpn. **51**, 263 (1999).